The effect of ocean acidification on tropical coral calcification: insights from calcification fluid DIC chemistry

Nicola Allison[*a], Catherine. Cole[a], Chris Hintz[b], Ken Hintz[c], James Rae[a], Adrian Finch[a]

*Corresponding author, email: na9@st-andrews.ac.uk

[a] School of Earth and Environmental Sciences, University of St. Andrews, St. Andrews KY16 9AL, UK

[b] Department of Marine and Environmental Sciences, Savannah State University, Savannah, GA USA

[c] Department of Electrical and Computer Engineering, George Mason University, Fairfax, VA, USA

Abstract

Ocean acidification typically reduces calcification in tropical marine corals but the mechanism for this process is not understood. We use skeletal boron geochemistry (B/Ca and $\delta^{11}B$) to reconstruct the calcification fluid DIC of corals cultured over both high and low seawater pCO_2 (180, 400 and 750 µatm). We observe strong positive correlations between calcification fluid pH and concentrations of the DIC species potentially implicated in aragonite precipitation (be they CO_3^{2-}, HCO_3^- or $HCO_3^-+CO_3^{2-}$). Similarly, with the exception of one outlier, the fluid concentrations of precipitating DIC species are strongly positively correlated with coral calcification rate. Corals cultured at high seawater pCO_2 usually have low calcification fluid pH and low concentrations of precipitating DIC, suggesting that a reduction in DIC substrate at the calcification site is responsible for decreased calcification. The outlier coral maintained high pH_{CF} and DIC_{CF} at high seawater pCO_2 but exhibited a reduced calcification rate indicating that the coral has a limited energy budget to support proton extrusion from the calcification fluid and meet other calcification demands. We find no evidence that increasing seawater pCO_2 enhances diffusion of CO_2 into the calcification site. Instead the overlying $[CO_2]$ available to diffuse into the calcification site appears broadly comparable between seawater pCO_2 treatments, implying that metabolic activity (respiration and photosynthesis) generates a similar $[CO_2]$ in the vicinity of the calcification site regardless of seawater pCO_2.

Keywords: B/Ca, dissolved inorganic carbon, coral, calcification, $\delta^{11}B$, calcification fluid

Declarations of interest: none

1. Introduction

Rising atmospheric CO_2 has fundamentally affected seawater carbonate chemistry, lowering seawater pH (Caldeira and Wickett, 2003; IPCC, 2013). Understanding the impact of these changes on coral biomineralisation is essential for predicting the future of coral reef ecosystems. Most laboratory and field studies indicate that coral calcification is reduced at lower seawater pH

(Erez et al., 2011), but it is unclear why this occurs. Multiple studies explore correlations between calcification rate and seawater dissolved inorganic carbon (DIC) chemistry e.g. [CO_3^{2-}], [HCO_3^-], pH and Ω (Marubini et al., 2001; Schneider and Erez 2006; Jury et al., 2009). However, coral aragonite does not precipitate directly from seawater but from an extracellular calcifying fluid which multiple techniques (microsensors, pH sensitive dyes and skeletal boron geochemistry) indicate has significantly different DIC chemistry to the surrounding seawater (Al Horani et al., 2003; Venn 2011; Allison et al., 2014, Cai et al., 2016). The calcification fluid is probably derived from seawater (Tambutte et al., 2012) and located between the coral tissue and underlying skeleton (Clode and Marshall, 2002). Corals actively increase the pH of the fluid above that of seawater (Al Horani et al., 2003; Venn et al., 2011, 2012; Cai et al., 2016). This may serve as a mechanism to concentrate DIC, one of the substrates required for aragonite precipitation (Allison et al., 2014). Increasing calcification fluid pH shifts the DIC equilibrium in favour of carbonate (CO_3^{2-}) at the expense of CO_2 and bicarbonate (HCO_3^-), creating a CO_2 concentration gradient between the fluid and the surrounding environment. CO_2 can diffuse into the calcification fluid and react to form more HCO_3^- and CO_3^{2-}, thereby increasing calcification fluid DIC (Erez 1978). Corals cultured at high seawater pCO_2 have lower calcification fluid pH than their counterparts cultured at low pCO_2 (Venn et al., 2012; McCulloch et al., 2012). This suggests that they are unable to concentrate DIC at the calcification site to the same extent and may explain the reduction in calcification rate.

The DIC chemistry of the coral calcification fluid can be estimated from the boron geochemistry of the coral skeleton (Allison et al., 2014, McCulloch et al., 2017, Ross et al., 2017). In brief, there is a large B isotope fractionation between the predominate dissolved boron species in seawater and borate, $B(OH)_4^-$, is depleted in ^{11}B compared to boric acid, $B(OH)_3$ (Kakihana et al., 1977). B speciation is controlled by ambient pH and the $\delta^{11}B$ of $B(OH)_4^-$ is therefore pH dependent. Since $B(OH)_4^-$ is predominantly incorporated into the aragonite lattice (Sen et al., 1994, Noireaux et al., 2015, Balan et al., 2016), skeletal $\delta^{11}B$ reflects calcification fluid pH while [B] reflects both fluid pH and the concentration of the DIC species competing with borate for inclusion in the carbonate (Allen et al., 2012).

In this study we have analysed the boron geochemistry of a suite of corals cultured over a range of seawater pCO_2, including concentrations both lower and higher than the present day. The application of coral boron geochemistry assumes that aragonitic boron predominately occurs in tetrahedral coordination (B4), likely as $B(OH)_4^-$ substituted for CO_3^{2-} (Balan et al., 2016). However Klochko et al. (2009) reported 36% of boron in trigonal co-ordination (B3) in the shallow tropical coral *Porites* spp. while Rollion Bard et al. (2011) identified 18% and 48% B3 in the skeletal fibres and centres of calcification respectively of a deep water coral. Klochko et al (2009) and Noireaux et al (2015) report good agreement between the observed aragonite $\delta^{11}B$ and that predicted from the incorporation of $B(OH)_4^-$, leading both to conclude that any B3 was initially incorporated as B4 and then underwent a coordination change whilst preserving the original $B(OH)_4^-$ isotopic signature. In contrast, in the deep sea coral, high B3 was associated with low $\delta^{11}B$ suggesting that $B(OH)_3$ was incorporated in the skeletal centres of calcification (Rollion Bard et al., 2011). During this research we avoided the analysis of centres of calcification and we assume that coral skeletal boron is derived from dissolved $B(OH)_4^-$. We cultured three different massive *Porites* spp. genotypes, cutting multiple colonies (each >12 cm in diameter) from coral heads to enable the study of large individuals of the same genotype over a range of seawater pCO_2. We reconstruct the DIC chemistry of the coral calcification fluids and correlate this with measured coral calcification rates

(Cole et al., 2018).

2. Methods and materials

2.1 Coral culturing

Large coral heads were collected from spatially separate (non-adjoining) massive *Porites* spp. colonies in Fiji and imported into the UK. We defined each massive colony as a separate genotype and divided each head into multiple pieces (each ~12 cm in diameter) to enable the culture of corals of the same genotype in each pCO_2 treatment. Corals were cultured in a purpose-built large-volume aquarium system constructed of low CO_2 permeability materials and designed to control temperature, salinity and dissolved inorganic carbon (DIC) system parameters within narrow limits (Cole et al., 2016, 2018). The corals were maintained in 21 l cast acrylic tanks, recirculated with seawater from high density polyethylene reservoirs containing ~900 litres of seawater. At the start of the experiment the reservoirs were filled with fresh artificial seawater (Red Sea Salt, Red Sea Aquatics, UK) seeded with artificial seawater from a mixed coral/fish aquarium. During tank cleaning, ~10-15 l of seawater was typically removed from each reservoir each week and was replaced with fresh artificial seawater. No seawater replacement occurred during the experimental period (see below).

The seawater in each treatment was bubbled with gas mixes set to reach the target seawater pCO_2 compositions. Corals were cultured at seawater pCO_2 of ~180 µatm (the CO_2 atmosphere during the last glacial maximum, Petit et al., 1999), ~400 µatm (the present day) and ~750 µatm (projected to occur by the end of the present century, IPCC 2013). Physical and chemical parameters of the culture seawater are summarised in Table 1. Seawater temperatures were measured hourly (TinyTag Aquatic, Gemini Data Loggers, UK) salinities were measured twice daily on 4 days of each week in the experimental periods (Thermo Orion 5 star meter, calibrated to NIST conductivity standards). Total alkalinity was measured by automated Gran titration (Metrohm, 888 Titrando) twice daily on 4 days of each week in the experimental periods. Precision of duplicate ~30 ml analyses was typically ±2 µeq kg^{-1}. The precision of multiple measurements of synthetic Na_2CO_3 standards was consistently ± 3 µeq kg^{-1} (1σ, between days). The total alkalinity, [Ca] and [Sr] of the culture seawater was maintained by additions of 0.6M Na_2CO_3 and a mixture of 0.58M $CaCl_2$ + 0.02M $SrCl_2$ by 200 µl volume solenoid diaphragm pumps, evenly spaced over a 24 hour period, controlled by a custom-written MATLAB® dosing control program. DIC was measured weekly in each reservoir using a CO_2 differential, non-dispersive, infrared gas analyser (Apollo SciTech; AS-C3). Samples were calibrated against a natural seawater certified reference material (CRM; A. Dickson, Scripps Institution of Oceanography). Internal reproducibility was calculated from the standard deviation of 8 replicate measurements of a single sample ($\sigma/\sqrt{n}$), and was always ≤0.1%. Multiple measurements of the CRM analysed as an unknown were in excellent agreement with the certified value (within 5 µmol kg^{-1}, Cole et al., 2016). Lighting of ~ 300 µmol photons m^{-2} s^{-1} was provided by Maxspect R420R 160w-10000k LED lamps on a 12h light: 12h dark cycle (with wavelength settings of 100% A and 20% B). Corals were fed weekly with frozen rotifers.

Corals were maintained at ambient pCO_2 conditions for 2 months, adjusted to pCO_2 treatment conditions over another 2 months and then acclimated at the final treatment pCO_2 for 5 months. Colonies were then stained with Alizarin Red S and cultured for a 5 week experimental period

before sacrifice. Light and dark colony calcification rates were estimated 3-4 times in this experimental period by isolating the colony for 5 (in the light) or 7 (in the dark) hours and using the alkalinity anomaly technique (Cole et al., 2018).

2.2 Seawater B/Ca and $\delta^{11}B$ analyses

Seawater samples were collected weekly during the experimental period and analysed for B and Ca by quadrupole ICP-MS (Thermo Scientific X Series) at the National Oceanography Centre, Southampton. Samples were diluted 1000-fold in 5% HNO_3 (with 5 ppb In as an internal standard) and calibrated against matrix-matched synthetic standards prepared from 1000 µg ml^{-1} single-element stock solutions (Inorganic Ventures) in 5% HNO_3. Replicate analyses (n = 4) of a standard seawater yielded a B/Ca standard deviation of 1.5%. Boron isotopes were separated from the seawater matrix by column chromatography and analysed on a Neptune Plus MC-ICPMS (Rae et al., 2011). The long-term reproducibility of these measurements is 0.2 ‰ (2 SD).

2.3 Skeletal $\delta^{11}B$ and B/Ca analyses

Corals were immersed in 3-4% sodium hypochlorite for ≥24 h with intermittent agitation to remove organic contamination, then rinsed repeatedly in distilled water and dried. Skeletal strips from the outermost surface of the colonies were sawn along the maximum growth axes and fixed in 25 mm epoxy resin blocks (Epofix, Struers Ltd.). Blocks were polished using silicon carbide papers (up to 4000 grade, lubricated with water) and polishing alumina (0.05 µm, suspended in water).

Skeletal $\delta^{11}B$ and B/Ca were determined by SIMS using a Cameca 1270 in the School of GeoSciences at the University of Edinburgh. The experimental period was identified from the Alizarin Red S stain and multiple SIMS analyses (n=17-24) were evenly spaced across this section of the skeleton in 2-5 different corallites of each colony. The high spatial resolution of SIMS allows the selective analysis of the small volumes of aragonite deposited in the experimental period and the avoidance of centres of calcification which appear as dark areas in reflected light when exposed on the section surface (Allison and Finch 2009). Sections were gold coated and analysed with a primary $^{16}O_2^-$ beam of ~ 7 nA, accelerated at 22 keV and focussed to an oval ~25 x 35 µm. Instrument conditions were energy offset = 0 eV (100 eV window), imaged field = 25 µm, entrance slits 150 µm and exit slits 500 µm (mass resolution was ~2400). Secondary ions were collected by a single electron multiplier and by cycling the magnetic field through the mass range. Singly-charged cations were collected at masses ^{10}B (11 seconds per cycle) and ^{11}B (3s) yielding typical count rates of ~1400 and 5300 cps respectively. Doubly charged $^{40}Ca^{2+}$ ions were collected at mass 20 (1s) and typical count rates were ~60000 cps. Each analysis is the sum of 60 cycles. A pre-analysis sputter time of 30 s in spot mode was used to remove surface contamination. Internal reproducibility (the precision at a single point) was calculated from the standard deviation (σ) of the 60 cycles in each coral analysis (σ/(√60)) and was typically 1.6‰. The precision (1σ) of multiple analyses of each coral sample was typically 1.4‰ ($\delta^{11}B$) and 9% (B/Ca).

All analyses were normalized to a *Porites* spp. coral standard ($\delta^{11}B$ = 24.8‰, B/Ca = 0.364 mmol mol^{-1}, Kasemann et al., 2009). Minor differences in the B/Ca and $\delta^{11}B$ of the SIMS coral standard and the chips of the same coral characterised by bulk methods may affect the accuracy of our SIMS estimates but our estimates of analytical precision are good. A

Desmophyllum spp. cold water coral chip ($\delta^{11}B \approx 16.7 \pm 1.2‰$ (1σ); B/Ca ≈ 0.15 mmol $mol^{-1} \pm 3\%$ (1σ), based on comparison with the coral standard) which exhibited limited heterogeneity in B/Ca and $\delta^{11}B$ was analysed to confirm that there was no instrumental drift within and between days. Multiple analyses were completed each day (n=9-13) to yield a 95% confidence limit of the mean $\delta^{11}B$ of the standard which was typically ~0.9‰ and was always better than ±1.2‰. 95% confidence limits of the mean B/Ca of the standard was always ≤±2.6%.

2.4 Calculation of calcification fluid DIC parameters

Equilibrium constants and their p*K* values were calculated from the known temperatures and salinity of the culture seawater in each treatment (Table 1.). Equilibrium constants for carbonic acid were calculated from Mehrbach et al. (1973), refit by Dickson and Millero (1987) and for $KHSO_4$ from Dickson (1990). E_{CF} pH was estimated from skeletal $\delta^{11}B$ as:

$$pH_{ECF} = pK_B - \log\left(-\frac{\delta^{11}B_{ECF} - \delta^{11}B_{skeleton}}{\delta^{11}B_{CF} - \alpha_B\,\delta^{11}B_{skeleton} - 1000(\alpha_B - 1)}\right) \quad (1)$$

using α_B (=1.0266, the mean of two empirical estimates (Klochko et al., 2006, Nir et al., 2015) and assuming that the $\delta^{11}B$ of the calcification fluid ($\delta^{11}B_{CF}$) is the same as culture seawater (Table 1).

Dissolved boron is transported into the calcification fluid in seawater and we infer that the total [B] of the fluid is the same as the seawater in each treatment (Table 1) and is constant (reflecting the very low partitioning of $B(OH)_4^-$ into aragonite, Allison et al. 2014). We assume that $[B(OH)_4^-]$ only partitions into aragonite and we used pH_{CF} to estimate $[B(OH)_4^-]_{CF}$:

$$K^*_B = \frac{[H^+]_{CF}\ [B(OH)_4^-]_{CF}}{[B(OH)_3]_{CF}} \quad (2)$$

$B/Ca_{skeleton}$ equates to $B/CO_3^{2-}{}_{skeleton}$ as Ca and C are equimolar in $CaCO_3$. We used $[B(OH)_4^-]_{CF}$, $B/Ca_{skeleton}$ and the relevant $B(OH)_4^-$/(co-precipitating DIC species) partition coefficient (K_D) to estimate the concentration of the DIC species co-precipitating with $B(OH)_4^-$ in the calcification fluid e.g. if $B(OH)_4^-$ co-precipitates with $[CO_3^{2-}]$ then:

$$B/Ca_{skeleton} = K_D B(OH)_4^-/CO_3^{2-} \quad x \quad \frac{[B(OH)_4^-]_{CF}}{[CO_3^{2-}]_{CF}} \quad (3)$$

K_D have been calculated for aragonite under a range of different scenarios (Allison et al., 2014, 2017, Mavromatis et al., 2015, Holcomb et al. 2016 and De Carlo et al., 2018). While it is likely that $B(OH)_4^-$ substitute for CO_3^{2-} in aragonite (Balan et al., 2016), it is unknown which aqueous DIC species are involved in aragonite precipitation. De Carlo et al (2018) conclude that insignificant correlations between fluid $[HCO_3^-]$ and precipitation rates of inorganic aragonites indicate that HCO_3^- is not involved in precipitation. However they did not utilise a seed in their experiments and they are unable to discriminate between the rates of $CaCO_3$ nucleation (likely controlled by CO_3^{2-}, Gebauer et al., 2008) and subsequent crystal growth. Both aqueous HCO_3^- and CO_3^{2-} are inferred to attach to growing calcite crystal surfaces with the HCO_3^- subsequently deprotonating to leave CO_3^{2-} preserved in the carbonate lattice (Wolthers et al., 2012). HCO_3^- is observed in both coral

and synthetic aragonite which may be a remnant of attached un-deprotonated HCO_3^- (Von Euw et al., 2017).

Holcomb et al (2016) identified an effect of saturation state on K_D in synthetic aragonites which complicates the interpretation of coral skeletal [B]. McCulloch et al., (2017) replotted the Holcomb et al. data to describe K_D as a function of precipitating fluid $[H^+]$ reasoning that $B(OH)_4^-$ likely deprotonates during substitution for CO_3^{2-} to preserve charge neutrality. However $B(OH)_4^-$ deprotonation is not supported by experimental NMR data (Balan et al., 2016) and charge neutrality during $B(OH)_4^-$ substitution for CO_3^{2-}, is likely accomplished by substitution of Na^+ for Ca^{2+} (Balan et al., 2016). Neither the De Carlo et al. (2018) or McCulloch et al., (2017) replots of the Holcomb dataset consider the large variations in $[Ca^{2+}]$ (x3) which occur in the Holcomb et al (2016) dataset and affect fluid saturation state.

Allison (2017) replotted the combined datasets of Mavromatis et al. (2015) and Holcomb et al (2016) for synthetic aragonites precipitated at 25°C to show that K_D is highly dependent on precipitating fluid saturation state. This may reflect enhanced incorporation of B during rapid crystal extension, as in calcite (Gabitov et al., 2014). However observed patterns in coral skeletal B/Ca can only be reproduced assuming that K_D is approximately constant (Allison, 2017). This apparent conflict can be resolved if changes in the coral calcification fluid saturation state are not associated with increases in crystal extension rate e.g. if increases in coral calcifying fluid saturation state are associated with increases in the numbers of aragonite crystals deposited rather than the extension rates of individual crystals (Allison, 2017).

In this study we utilize the $B(OH)_4^-$/precipitating DIC aragonite partition coefficients calculated in Allison (2017) from the Holcomb et al (2016) dataset. We assume $B(OH)_4^-$ substitutes into aragonite for either CO_3^{2-} only, HCO_3^- only or both $HCO_3^-+CO_3^{2-}$ and apply $B(OH)_4^-/CO_3^{2-}$, $B(OH)_4^-/HCO_3^-$ and $B(OH)_4^-/(CO_3^{2-}+HCO_3^-)$ partition coefficients of $1.05x10^{-3}$, $6.36x10^{-3}$ and $6.99x10^{-3}$ respectively (Allison, 2017). We note that fluid saturations states within single aragonite precipitations in the Holcomb study are highly variable ($[Ca^{2+}]$ typically varies by up to x3, while [DIC] varies by up to x 4) and we consider that the calculated partition coefficients should be treated as broad approximations only.

3. Results

Seawater and skeletal B/Ca and $\delta^{11}B$ data are summarised in Table 1. In all treatments, seawater [B] is close to natural values but $\delta^{11}B$ is ~-1‰. Commercial sea salts are formed from the evaporation of seawater resulting in the removal of B in the water vapour phase (Gast and Thompson, 1959). Boron is replenished by the addition of boric acid yielding the high seawater $\delta^{11}B$ observed here.

We report all pH on the total scale and use the subscript $_{CF}$ to denote the DIC characteristics of the calcification fluid. We calculate fluid DIC assuming that $B(OH)_4^-$ co-precipitates with HCO_3^- and/or CO_3^{2-} and we express concentrations as $[CO_3^{2-}]_{CF}$ (assuming that CO_3^{2-} only is utilized during aragonite precipitation), $[HCO_3^-]_{CF}$ (assuming that HCO_3^- only is utilized during aragonite precipitation) and $[HCO_3^-+CO_3^{2-}]_{CF}$ (assuming that both $HCO_3^-+CO_3^{2-}$ are utilized). We use the term [co-precipitating DIC] to discuss observations which apply to all of these precipitation scenarios. We cultured and analysed two duplicate colonies of the *P. murrayensis* genotype at 400 and

750 µatm seawater pCO_2 (Table 1). We observed significant variations in pH_{CF} (2 tailed t test, p=0.05) between both duplicates although in only one case (at 750 µatm) was this associated with a significant difference in [co-precipitating DIC]$_{CF}$.

All corals increased pH_{CF} (Fig. 1a) above that of seawater (Table 1). All corals cultured at 180 µatm exhibited significantly higher pH_{CF} than their analogues at 400 µatm and 750 µatm but pH_{CF} did not vary significantly between 400 µatm and 750 µatm in any coral genotype (Table 2). pH_{CF} and [co-precipitating DIC]$_{CF}$ exhibit a broad positive correlation under all co-precipitation scenarios (Fig 1b, r^2=0.57, p=0.008). Replotting this figure to discriminate between coral species, produces stronger coefficients of determination (Figure 2) and indicates that [co-precipitating DIC] is more concentrated in *P. murrayensis* than in *P. lutea* for a comparable pH_{CF}, yielding [CO_3^{2-}]$_{CF}$ and [HCO_3^-+CO_3^{2-}]$_{CF}$ values which are typically higher by ~70 µmol kg^{-1} and ~400 µmol kg^{-1} respectively.

4. Discussion

4.1 Calcification fluid DIC chemistry

Regardless of the co-precipitating DIC species, pH_{CF} and [co-precipitating DIC]$_{CF}$ are positively correlated in each coral species (Figure 2). The opposite trend has been observed between seasonal variations in pH_{CF} and [DIC]$_{CF}$ in modern corals from Australia (McCulloch et al., 2017, Ross et al., 2017). Seasonal variations in ambient seawater pH, temperature and light likely impact coral carbon metabolism (photosynthesis and respiration), enzyme activities (e.g, Ca-ATPase pumping out of the calcification fluid) and calcification (which decreases pH_{CF}). These confounding effects do not occur in the present study enabling us to isolate the impact of seawater pCO_2 on calcification fluid chemistry.

Our data indicate that increases in pH_{CF} act to concentrate co-precipitating DIC at the calcification site. Increasing pH_{CF} drives the DIC equilibrium to reduce calcification fluid [CO_2] and probably creates a CO_2 concentration gradient between the fluid and the surroundings i.e. coral tissues and local seawater, which are separated from the fluid by a permeable membrane. We note that corals of each species fall along a common line, describing pH_{CF} and [co-precipitating DIC]$_{CF}$, regardless of seawater pCO_2 treatment. To emphasize the importance of this we illustrate the [co-precipitating DIC] of a seawater based fluid as a function of pH under two different CO_2 diffusion scenarios. In the first scenario we assume that the system is fully open and that CO_2 diffuses readily from the surroundings into the fluid to maintain an equilibrium with local seawater. CO_2 diffusing into the calcification site predominantly converts to HCO_3^- and CO_3^{2-} and all [co-precipitating DIC]$_{CF}$ are positively correlated with pH_{CF} (Fig 3a-c). In the second scenario we assume that CO_2 diffuses into the system as in the open system but that the rate of diffusion is a function of the CO_2 concentration gradient (ΔC_w) between the fluid and the seawater (see Allison, 2017 for full details and a sample calculation). We estimate the concentration gradient by assuming that the [CO_2] of the calcification fluid reflects that of ambient seawater brought to pH_{CF} and that seawater [CO_2] is the same as ambient seawater in each pCO_2 treatment (Fig. 4). We arbitrarily assume that CO_2 diffusion doubles the [DIC]$_{CF}$ at pH 8.5 in the 400 µatm CO_2 scenario (as in Allison 2017) and scale the addition of DIC to the calcification fluid over the full fluid pH in all pCO_2 treatments as a linear function of this ΔC_w (Fig 3d-f). Although CO_2 invasion is more limited in this second set of calculations (Allison 2017), both scenarios predict large variations in [co-precipitating DIC]$_{CF}$

between different seawater pCO_2 treatments.

These predictions are in marked contrast with our observed data (overlain onto Fig 3). The coral data implies that the concentration of co-precipitating DIC in the calcification fluid is not affected by changes in seawater pCO_2 between treatments i.e. increasing seawater pCO_2 does not impact the CO_2 available to diffuse into the calcification site (Hohn and Merico, 2012). Rather our data suggests that the overlying $[CO_2]$ available to diffuse into the calcification site is broadly comparable between treatments implying that metabolic activities (respiration and photosynthesis) generates a similar $[CO_2]$ in the vicinity of the calcification site regardless of seawater pCO_2.

$[\text{Co-precipitating DIC}]_{CF}$ is higher in *P. murrayensis* than in *P. lutea* for a comparable pH_{CF} (Fig. 2) Trace element partitioning into carbonates may be affected by mineral precipitation rate due to Rayleigh fractionation (Elderfield et al., 1996) or growth entrapment (Watson, 1994) but calcification rates for the 2 coral species are broadly comparable (Cole et al., 2018) and it is unlikely that this accounts for the offset in $[DIC]_{CF}$. The more effective concentration of DIC in *P. murrayensis* could reflect a greater activity of bicarbonate anion transporters (Tambutte et al., 1996; Zoccola et al., 2015) in this species or a higher tissue $[CO_2]$ which enables a greater diffusion of CO_2 into the calcification site (Erez 1978).

pH_{CF} varied significantly between duplicate colonies of the *P. murrayensis* at 400 µatm and 750 µatm. Water in the tanks was well mixed and duplicate differences do not reflect temperature, seawater pCO_2 or nutrient levels. Similarly light variations over the tank footprint were small and photosynthetically active radiation light varied by 250-300 µmol photons m^{-2} s^{-1}. The $\delta^{11}B$ of massive corals has been applied as a proxy of past and modern seawater pH and to indicate air:sea carbon flux (Pelejero et al., 2005; Shinjo et al., 2013; Kubota et al., 2014). The high pH_{CF} variability observed between corals cultured at the same seawater pCO_2 (even for prolonged periods of>9 months) suggests that it will be difficult to estimate past seawater pH accurately from fossil coral $\delta^{11}B$.

4.2 Calcification fluid DIC chemistry and calcification rate

We plotted calcification rate (from Cole et al 2018) against $[CO_3^{2-}]_{CF}$ and $[HCO_3^{-}+CO_3^{2-}]_{CF}$ for each coral genotype (Fig. 5a). Assuming that calcification fluid $[Ca^{2+}]$ is similar to that of seawater (Al Horani et al., 2003), this is effectively a measure of the saturation state of the calcification fluid. We observe excellent correlations between $[CO_3^{2-}]_{CF}$ and $[HCO_3^{-}+CO_3^{2-}]_{CF}$ and calcification rate in both *P. lutea* genotypes although we found the two genotypes exhibit markedly different relationships. *P. lutea* 1 attains higher calcification rates than *P. lutea* 2, at comparable values of $[CO_3^{2-}]_{CF}$ or $[HCO_3^{-}+CO_3^{2-}]_{CF}$, particularly at the lower ends of the DIC_{CF} ranges. Clearly calcification rate variations between genotypes do not solely reflect calcification fluid DIC chemistry. Coral skeletons include soluble and insoluble organic materials which are present at the calcification site and/or are subsequently embedded in the skeleton (Clode and Marshall, 2002; Falini et al., 2013). These organic materials are implicated in the catalysis of crystallization and mediation of the skeletal architecture. For example, individual proteins, isolated from coral skeletal materials, can spontaneously catalyse the precipitation of aragonite at pH similar to that of seawater (Mass et al., 2013). The skeletal organic matrix amino acid composition varies between coral species (Van de Locht, 2014) and between corals of different growth rates (Falini et al., 2013). We hypothesise that the two *P. lutea* genotypes produce different skeletal organic materials which impact the

precipitation rates of their respective skeletons.

The third coral genotype, *P. murrayensis*, also exhibits an excellent relationship between [co-precipitating DIC]$_{CF}$ and calcification rate with the exception of one point (Fig. 5a). Calcification rates for this outlier were highly variable (note the large standard deviation of this mean). Skeletal chemistry predominantly reflects the higher rate of variable calcification (in this case 14.1 mmol $CaCO_3$ cm^{-2} day^{-1}), when most of the analysed skeleton was deposited, but even after accounting for this, the calcification rate of this outlier coral is lower than that expected from the [co-precipitating DIC]$_{CF}$ versus calcification rate relationship observed in the other colonies of this genotype. Plotting calcification rate as a function of the H^+ concentration gradient between the calcification fluid and the surrounding seawater produces strong inverse correlations in each genotype which span all coral samples with no outliers (Fig. 5b). Coral calcification is likely to be energetically expensive (Allemand et al., 2011) requiring synthesis of the skeletal organic matrix to guide precipitation of the skeleton and ion transport e.g. H^+ extrusion from the calcification site by Ca-ATPase (Al Horani et al., 2003). We hypothesise that the outlier coral in Fig. 5a may expend a large proportion of its energy budget in maintaining a relatively high pH_{CF} at the expense of synthesis of the skeletal organic matrix resulting in a low calcification rate for this individual.

4.3 Implications for biomineralisation and ocean acidification

With the exception of the outlier, corals cultured at high seawater pCO_2 had low pH_{CF} and DIC_{CF}. In our dataset the calcification fluid pH increase is fundamental in concentrating precipitating DIC for calcification (Fig 1b). While it is not clear which DIC species is/are utilised in aragonite precipitation calcification rate is usually strongly dependent on [co-precipitating DIC]$_{CF.}$ This suggests that the decreased calcification rates typically observed in corals cultured at high seawater pCO_2 (Erez et al., 2011) reflect a reduced ability to concentrate DIC at the calcification site. Corals cultured at high seawater pCO_2 may remove more protons from the calcification fluid than their lower seawater pCO_2 analogues, partially offsetting the effects of ocean acidification, but they do not usually attain the same high pH_{CF} (Venn et al., 2012) and probably do not accumulate DIC_{CF} to the same extent. Corals cultured at low seawater pH may upregulate genes coding for bicarbonate anion transport (Vidal-Dupiol et al., 2013) but, if this occurred in our samples, it did not compensate for the decrease in calcification fluid DIC.

One coral in our datatset continued to attain high pH_{CF} and DIC_{CF} at high seawater pCO_2 but in this case the coral exhibited a reduced calcification rate suggesting that the coral has a limited energy budget to support proton extrusion from the calcification fluid and meet other calcification demands. We infer that future increases in atmospheric CO_2 (and concurrent decreases in seawater pH) will likely decrease both coral pH_{CF} and [DIC]$_{CF}$ and ultimately reduce coral calcification.

Conclusions

Calcification fluid pH and [co-precipitating DIC] estimates from skeletal $\delta^{11}B$ and B/Ca are positively correlated in all corals. Corals cultured at high seawater pCO_2 usually have relatively low fluid pH and [precipitating DIC]. [Precipitating DIC] and coral calcification rate are positively correlated in all but one outlier coral and reduced DIC substrate at the calcification site is the likely

cause of decreased coral calcification rates under ocean acidification scenarios. The outlier coral maintained a high calcification fluid pH and [co-precipitating DIC] at high seawater pCO_2 but exhibited a low calcification rate suggesting that corals have a limited energy budget for calcification which is apportioned between proton extrusion from the calcification site and other processes e.g. synthesis of the skeletal organic matrix.

Acknowledgements

This work was supported by the UK Natural Environment Research Council (award NE/I022973/1) to AAF and NA. NERC Scientific Services provided access to the ion microprobe, and we are indebted to Richard Hinton (EIMF, University of Edinburgh) for his assistance with the analyses. Seawater B/Ca analyses were carried out by Matt Cooper (University of Southampton). We thank Dave Steven, Mark Robertson, Casey Perry, Mike Scaboo and Andy Mackie for their assistance with the culture system build.

References

Al-Horani, F.A., Al-Moghrabi, S.M., de Beer, D., 2003. The mechanism of calcification and its relation to photosynthesis and respiration in the scleractinian coral *Galaxea fascicularis*. Mar. Biol. 142, 419-426.

Allen, K.A., Honisch, B., Eggins, S.M., Rosenthal, Y., 2012. Environmental controls on B/Ca in calcite tests of the tropical planktic foraminifer species *Globigerinoides ruber* and *Globigerinoides sacculifer*. Earth Planet. Sci. Lett. 351-352, 270-280.

Allison, N., 2017. Reconstructing coral calcification fluid dissolved inorganic carbon chemistry from skeletal boron: an exploration of potential controls on coral aragonite B/Ca. Heliyon, 3, https://doi.org/10.1016/j.heliyon.2017.e00387.

Allison, N., Cohen, I., Finch, A.A., Erez, J., Tudhope, A.W., 2014. Corals concentrate dissolved inorganic carbon to facilitate calcification. Nat. Commun. 5, 5741, https://doi.org/10.1038/ncomms6741.

Allison, N., Finch, A.A., 2009. Reproducibility of minor and trace element determinations in Porites coral skeletons by secondary ion mass spectrometry, Geochem. Geophys. Geosyst., 10, Q04003, https://doi.org/10.1029/2008GC002239.

Allemand, D., Tambutte, E., Zoccola, D., Tambutte S., 2011. Coral Calcification, Cells to Reefs. In *Coral Reefs: An Ecosystem in Transition (eds* Z. Dubinksy and N. Stambler). Springer Science, New York. pp. 119-150.

Balan, E., Pietrucci, F., Gervais, C., Blanchard, M., Schott, J., Gaillardet, J., 2016. First-principles study of boron speciation in calcite and aragonite, Geochim. Cosmochim. Acta, 193, https://doi.org/10.1016/j.gca.2016.07.026.

Cai, W.-J., Ma, Y., Hopkinson, B.M., Grottoli, A.G., Warner, M.E., Ding, Q., Hu, X., Yuan, X., Schoepf, V., Xu, H., Han, C., Melman, T.F., Hoadley, KD., Pettay, D.T., Matsui, Y., Baumann, J. H., Levas, S., Ying, Y., Wang, Y. 2016. Microelectrode characterization of coral daytime interior pH and carbonate chemistry. Nat. Commun. 7, 11144; https://doi.org/10.1038/ncomms11144.

Caldeira, K., Wickett, M.E., 2003. Anthropogenic carbon and ocean pH. Nature 425, 365–365.

Clode, P.L., Marshall, A.T., 2002. Low temperature FESEM of the calcifying interface of a scleractinian coral. Tissue and Cell 34, 187-198.

Cole, C., Finch, A.A., Hintz, C., Hintz, K., Allison, N. 2016. Understanding cold bias: variable response of skeletal Sr/Ca to seawater pCO_2 in acclimated massive *Porites* corals, Scientific

Reports 6, 26888; https://doi.org/10.1038/srep26888.

Cole, C., Finch, A.A., Hintz, C., Hintz, K., Allison, N., 2018. Effects of seawater pCO_2 and temperature on calcification and productivity in the coral genus *Porites* spp.: an exploration of potential interaction mechanisms, Coral Reefs, https://doi.org/10.1007/s00338-018-1672-3.

DeCarlo, T.M., Holcomb, M., McCulloch, M.T., 2018. Reviews and syntheses: Revisiting the boron systematics of aragonite and their application to coral calcification, Biogeosciences, 15, 2819-2834, https://doi.org/10.5194/bg-15-2819-2018.

Dickson, A.G., 1990. Standard potential of the reaction: $AgCl(s) + 12H_2(g) = Ag(s) + HCl(aq)$ and the standard acidity constant of the ion HSO_4^- in synthetic sea water from 273.15 to 318.15K. J. Chem. Thermodynamics 22,113-127.

Dickson, A.G., Millero, F.J., 1987. A comparison of the equilibrium constants for the dissociation of carbonic acid in seawater media. Deep-Sea Research, 34, 1733-1743.

Elderfield, H., Bertram, C.J., Erez, J., 1996. Biomineralization model for the incorporation of trace elements into foraminiferal calcium carbonate. Earth Planet. Sci. Lett. 142, 409-423.

Erez, J. 1978. Vital effect on the stable-isotope composition seen in foraminifera and coral skeletons. Nature 273, 199-202.

Erez, J., Reynaud, S., Silverman, J., Schneider, K., Allemand, D., 2011. Coral calcification under ocean acidification and global change. In *Coral Reefs: An Ecosystem in Transition (eds* Z. Dubinksy and N. Stambler). Springer Science, New York. pp. 151-176.

Falini, G., Reggi, M., Fermani, S., Sparla, F., Goffredo, S., Dubinsky, Z., Levi, O., Dauphin, Y., Cuif J.-P., 2013. Control of aragonite deposition in colonial corals by intra-skeletal macromolecules. J. Struct. Biol. 183, 226-238.

Gabitov, R.I., Rollion-Bard, C. Tripati, A., Sadekov, A., 2014. In situ study of boron partitioning between calcite and fluid at different crystal growth rates, Geochimica et Cosmochimica Acta, 137, 81-92 https://doi.org/10.1016/j.gca.2014.04.014.

Gast, J.A., Thompson, T.G., 1959. Evaporation of boric acid from seawater, Tellus, 11, 344-347 https://doi.org/10.1111/j.2153-3490.1959.tb00039.x.

Gebauer, D., Volkel, A., Colfen, H., 2008. Stable prenucleation calcium carbonate clusters, Science, 322, 1819–1822.

Hohn, S., Merico, A., 2012. Modelling coral polyp calcification in relation to ocean acidification. Biogeosciences 9, 4441-4454.

Holcomb, M., DeCarlo, T.M., Gaetani, G.A., McCulloch, M., 2016. Factors affecting B/Ca ratios in synthetic aragonite. Chem. Geol. 437, 67-76.

IPCC Climate Change 2013, 2013. The Physical Science Basis. (eds T.F. Stocker and D.Qin) Cambridge Univ. Press, Cambridge, U.K.

Jury, C.P., Whitehead, R.F., Szmant, A.M., 2010. Effects of variations in carbonate chemistry on the calcification rates of *Madracis auretenra* (= *Madracis mirabilis sensu* Wells, 1973): bicarbonate concentrations best predict calcification rates, Global Change Biology, 16, 1632-1644.

Kakihana, K., Kotaka, M., Satoh, S., Nomura, M., Okamoto, M. 1977. Fundamental studies on ion exchange separation of boron isotopes, Bull. Chem. Soc. Japan, 50, 158-163.

Kasemann, S.A., Schmidt, D.N., Bijma, J., Foster, G.L., 2009. In situ boron isotope analysis in marine carbonates and its application for foraminifera and palaeo-pH. Chem. Geol. 260, 138-147.

Klochko, K., Kaufman, A.J., Yao, W.S., Bryne, R.H., Tossell, J. A., 2006. Experimental measurement of boron isotope fractionation in seawater. Earth Planet. Sci. Lett. 248, 276-285.

Klochko, K., Cody, G., Tossell, J.A., Dera, P., Kaufman, A.J., 2009. Re-evaluating boron speciation in biogenic calcite and aragonite using B-11, Geochim. Cosmochim. Ac, 73, 1890-1900.

Kubota, K., Yokoyama, Y., Ishikawa, T., Obrochta, S., Atsushi, S., 2014. Larger CO_2 source at the equatorial Pacific during the last deglaciation. Scientific Reports, https://doi.org/10.1038/srep05261.

Marubini, F., Barnett, H., Langdon, C., Atkinson, M.J., 2001. Dependence of calcification on light and carbonate ion concentration for the hermatypic coral *Porites compressa*. Mar. Ecol. Prog. Ser. 220:153–162.

Mass, T., Drake, J.L., Haramaty, L., Kim, J.D., Zelzion, E., Bhattacharya, D., Falkowski, P.G., 2013. Cloning and characterization of four novel coral acid-rich proteins that precipitate carbonates in vitro. Current Biology 23, 1126-1131.

Mavromatis, V., Montouillout, V., Noireaux, J., Gaillardet, J., Schott, J., 2015. Characterization of boron incorporation and speciation in calcite and aragonite from co-precipitation experiments under controlled pH, temperature and precipitation rate. Geochim. Cosmochim. Acta 150, 299-313.

McCulloch, M.T., Falter, J., Trotter, J., Montagna, P., 2012. Coral resilience to ocean acidification and global warming through pH up-regulation, Nature Climate Change, 2, 623–627.

McCulloch, M.T., D'Olivio, Falter, J. , Holcomb, M., Trotter, J., 2017. Coral calcification in a changing World and the interactive dynamics of pH and DIC upregulation, Nature Communications, 8, https://doi.org/10.1038/ncomms15686.

Mehrbach, C., Culberson, C.H., Hawley, J.E., Pytkowicx, R.M., 1973. ,Measurement of the apparent dissociation constants of carbonic acid in seawater at atmospheric pressure. Limnology and Oceanography, 18, 897-907.

Nir, O., Vengosh, A., Harkness, J.S., Dwye,r G.S., Lahav, O., 2015. Direct measurement of the boron isotope fractionation factor: Reducing the uncertainty in reconstructing ocean paleo-pH, Earth and Planetary Science Letters 414, 1-5.

Noireaux, J., Mavromatis, V., Gaillardet, J., Neuville, D., 2015. Crystallographic control on the boron isotope paleo-pH proxy. Earth Planetary Sci. Lett. 430, 398-407.

Pelejero, C., Calvo, E., McCulloch, M. T., Marshall, J. F., Gagan, M.K., Lough, J.M., Opdyke, B.N., 2005. Preindustrial to modern interdecadal variability in coral reef pH. Science, 309, 2204–2207.

Petit, J.R., Jouzel, J., Raynaud, D., Barkov, N.I., Barnola, J.-M., Basile, I., Bender, M., Chappellaz, J., Davis, M., Delaygue, G., Delmotte, M., Kotlyakov, V.M., Legrand, M., Lipenkov, V.Y., Lorius, C., PÉpin, L., Ritz, C., Saltzman, E., Stievenard, M., 1999. Climate and atmospheric history of the past 420 ky from the Vostok ice core, Antarctica. Nature 399, 429-436.

Rae, J.W.B., Foster, G.L., Schmidt, D.N., Elliott, T., 2011. Boron isotopes and B/Ca ratios in benthic foraminifera: proxies for the deep ocean carbonate system. Earth Planet. Sci. Lett. 302, 404-413 (2011).

Rollion-Bard, C., Blamart, D., Trebosc, J., Tricot, G., Mussi, A., Cuif J.P., 2011. Boron isotopes as pH proxy: a new look at boron speciation in deep-sea corals using 11B MAS NMR and EELS, Geochimica et Cosmochimica Acta 75, 1003-1012

Ross, C.L., Falter, J.L., McCulloch, M.T., 2017. Active modulation of the calcifying fluid carbonate chemistry (δ11B, B/Ca) and seasonally invariant coral calcification at sub-tropical limits, Scientific Reports, 7, https://doi.org/10.1038/s41598-017-14066-9.

Schneider, K., Erez, J., 2006. The effect of carbonate chemistry on calcification and photosynthesis in the hermatypic coral *Acropora eurystoma*. Limnol.. Oceanogr. 51, 1284-1293.

Sen, S., Stebbins, J.F., Hemming, N.G., Ghosh, B., 1994. Coordination environments of B-impurities in calcite and aragonite polymorphs - a B-11 mas NMR-study. Am. Mineralogist 79, 819-825.

Shinjo, R., Asami, R., Huang, K.-F., You, C.F., Iryu, Y., 2013. Ocean acidification trend in the tropical North Pacific since the mid-20th century reconstructed from a coral archive. Mar. Geol. 342, 58-64.

Tambutte, E., Allemand, D., Mueller, E., Jaubert, J., 1996. A compartmental approach to the mechanism of calcification in hermatypic corals. J. Exp. Biol. 199, 1029–41.

Tambutte, E., Tambutté, S., Segonds, N., Zoccola, D., Venn, A., Erez, J., Allemand D., 2012. Calcein labelling and electrophysiology: insights on coral tissue permeability and calcification. Proc. Royal Soc. B 279, 19-27.

Van de Locht, R., 2014. On the nanostructure of biogenic and bio-inspired calcium carbonate, PhD thesis, University of York, UK.

Venn, A.A., Tambutte, E., Holcomb, M., Allemand, D., Tambutte, S., 2011. Live tissue imaging shows reef corals elevate pH under their calcifying tissue relative to seawater. PLoS ONE 6, e20013.

Venn, A.A., Tambutte, E., Holcomb, M., Tambutte, S., 2012. Impact of seawater acidification on pH at the tissue-skeleton interface and calcification in reef corals. Proc. Natl. Acad. Sci. 110, 1634-1639.

Vidal-Dupiol, J., Zoccola, D., Tambutte, E., Grunau, C., Cosseau, C., Smith, K.M., Freitag, M., Dheilly, N.M., Allemand, D., Tambutte, S., 2013. Genes related to ion-transport and energy production are upregulated in response to CO_2-driven pH decrease in corals: new insights from transcriptome analysis. PLoS One 8, e58652; https://doi.org/10.1371/journal.pone.0058652.

Von Euw, S., Zhang, Q., Manichev, V.,Murali, N., Gross, J., Feldman, L.C., Gustafsson, T., Flach, C., Mendelsohn, R., Falkowski, P.G., 2017. Biological control of aragonite formation in stony corals. Science, 356, 933-938. https://doi.org/10.1126/science.aam6371.

Watson, E., 1994. A conceptual model for near-surface kinetic controls on the trace-element and stable isotope composition of abiogenic calcite crystals. Geochim. Cosmochim. Acta 68, 1473-1488.

Wolthers, M., Nehrke, G., Gustafsson, J.P., Van Cappellen, P., 2012.Calcite growth kinetics: Modelling the effect of solution stoichiometry. Geochim, Cosmochim, Acta 77, 121-134.

Zoccola, D., Ganot, P., Bertucci, A., Caminiti-Segonds, N., Techer, N., Voolstra, C.R., Aranda, M., Tambutté, E., Allemand, D., Casey, J.R., Tambutté, S., 2015. Bicarbonate transporters in corals point towards a key step in the evolution of cnidarian calcification. Sci. Rep. 5, 9983; https://doi.org/10.1038/srep09983.

Author contributions

NA and AAF conceived and designed the experiment, NA, AAF, KH and CH built the culturing system, NA and CC cultured and analysed the corals, CC and JR analysed the seawater $\delta^{11}B$, NA analysed the data and wrote the manuscript. All authors read and approved the manuscript.

Competing Financial Interests

The authors declare no competing financial interests.

Table 1. Physical and chemical characteristics of the seawater and coral skeletons in each treatment, measured over the 5-week experimental period. Seawater values are mean ± standard deviation (1σ) of n measurements. Dissolved inorganic carbon (DIC) and total alkalinity measurements were used to calculate seawater pH(total) using CO_2sys and equilibrium constants for carbonic acid (Mehrbach et al., 1973), refit by Dickson and Millero (1987) and HSO_4 (Dickson, 1990). Skeletal $\delta^{11}B$ and B/Ca are means ± 95% confidence limits. Calcification rates (μmol $CaCO_3$ cm^{-2} day^{-1}) are means ± standard deviations. Duplicates of the *P. murrayensis* genotype were cultured at 417 and 750 μatm and the values measured for each colony are shown separately.

		Seawater pCO_2		
		180 μatm	400 μatm	750 μatm
Seawater characteristics				
Temperature (°C)		25.3 ± 0.1	25.2 ± 0.2	25.1 ± 0.2
Salinity		35.1 ± 0.04	35.2 ± 0.08	35.2 ± 0.05
Total alkalinity (μmol kg^{-1})		2289 ± 14 (n=16)	2290 ± 8 (n=16)	2293 ± 5 (n=16)
Total DIC (μmol kg^{-1})		1831 ± 11 (n=5)	1999 ± 8 (n=5)	2113 ± 11 (n=5)
Seawater pH (total scale)		8.28	8.03	7.81
Seawater [B] (μmol kg^{-1})		392 ± 8 (n=5)	395 ± 6 (n=5)	405 ± 8 (n=5)
Seawater [Ca] (mmol kg^{-1})		9.78 ± 0.08 (n=5)	9.84 ± 0.10 (n=5)	9.86 ± 0.07 (n=5)
Seawater $\delta^{11}B$ (‰)		-1.07 ± 0.20 (n=4)	-0.90 ± 0.11 (n=3)	-1.00 ± 0.15 (n=3)
Skeleton characteristics				
Calcification rate	*P. lutea 1*	20.8 ± 0.6 (n=3)	18.9 ± 1.0 (n=4)	17.8 ± 2.6 (n= 4)
	P. lutea 2	21.3 ± 2.9 (n=3)	9.86 ± 2.0 (n=2)	4.22 ± 1.2 (n=3)
	P. murrayensis	22.8 ± 0.8 (n=3)	16.7 ± 0.8 (n=2)	9.30 ± 4.3 (n=3)
			15.0 ± 1.1 (n=3)	11.0 ± 1.5 (n=3)
$\delta^{11}B$	*P. lutea 1*	-16.0 ± 0.6 (n=17)	-17.5 ± 0.5 (n=21)	-17.0 ± 0.4 (n=22)
	P. lutea 2	-15.0 ± 0.8 (n=21)	-17.0 ± 0.7 (n=21)	-18.0 ± 0.7 (n=20)
	P. murrayensis	-14.6 ± 0.7 (n=24)	-16.5 ± 0.7 (n=18)	-15.8 ± 0.5 (n=19)
			-17.5 ± 0.4 (n=21)	-18.1 ± 0.5 (n=19)
B/Ca	*P. lutea 1*	0.367 ± 0.011 (n=17)	0.340 ± 0.018 (n=2))	0.398 ± 0.019 (n=22)
	P. lutea 2	0.360 ± 0.016 (n=21)	0.367 ± 0.008 (n=21)	0.381 ± 0.009 (n=20)
	P. murrayensis	0.343 ± 0.016 (n=24)	0.329 ± 0.011 (n=18)	0.316 ± 0.014 (n=19)
			0.306 ± 0.014 (n=21)	0.317 ± 0.015 (n=19)
pH_{CF} Total scale	*P. lutea 1*	8.50 ± 0.04 (n=17)	8.39 ± 0.03 (n=2))	8.42 ± 0.02 (n=22)
	P. lutea 2	8.56 ± 0.05 (n=21)	8.43 ± 0.04 (n=21)	8.36 ± 0.05 (n=20)
	P. murrayensis	8.58 ± 0.04 (n=24)	8.46 ± 0.04 (n=18)	8.51 ± 0.03 (n=19)
			8.39 ± 0.03 (n=21)	8.35 ± 0.04 (n=19)

Table 2. . Summary of significant differences (p=≤0.05 one way ANOVA followed by Tukey's pairwise comparisons) in pH_{CF} (estimated from skeletal $\delta^{11}B$) between individuals of the same coral genotype in different seawater pCO_2 treatments (180, 400 or 750 µatm). Data from duplicate corals are combined for this analysis.

	pH_{CF}
Genotype 1 (P. lutea)	180 > 400 180 > 750 400 = 750
Genotype 2 (P. lutea)	180 > 400 180 > 750 400 = 750
Genotype 3 (P. murrayensis)	180 > 400 180 > 750 400 = 750

Figure 1. a) Coral pH_{CF} (estimated from skeletal $\delta^{11}B$), and b) relationship between pH_{CF} and $[CO_3^{2-}]_{CF}$, assuming CO_3^{2-} only is utilized in calcification and $[HCO_3^- + CO_3^{2-}]_{CF}$, assuming both HCO_3^- and CO_3^{2-} are utilized in calcification (both μmol kg^{-1}). $[HCO_3^-]_{CF}$, assuming HCO_3^- only is utilized in calcification, is not shown but exhibits the same distribution with $[HCO_3^-]_{CF}$ spanning 2472-3659μmol kg^{-1}). Symbols denote coral genotypes and colours denote seawater pCO_2 treatment. pHCF error bars are calculated from 95% confidence limits of skeletal $\delta^{11}B$ analyses while $[CO_3^{2-}]_{CF}$, and $[HCO_3^- + CO_3^{2-}]_{CF}$ error bars are calculated from propagating 95% confidence limits in B/Ca and δ11B analyses onto DIC system estimates.

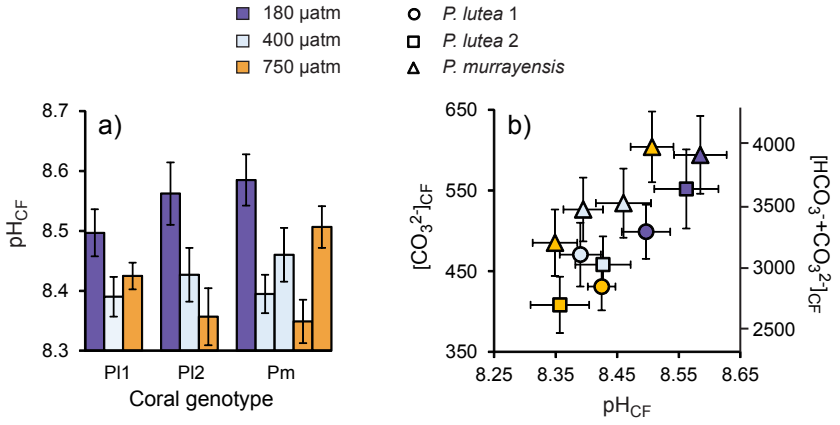

Figure 2. Correlations between pHCF and $[CO_3^{2-}]_{CF}$ and $[HCO_3^- + CO_3^{2-}]_{CF}$ (both μmol kg^{-1}) for all corals by species. For explanation of error bars see Figure 1. Coefficients of determination (r^2) for P. lutea and P. murrayensis are 0.84 and 0.83 respectively.

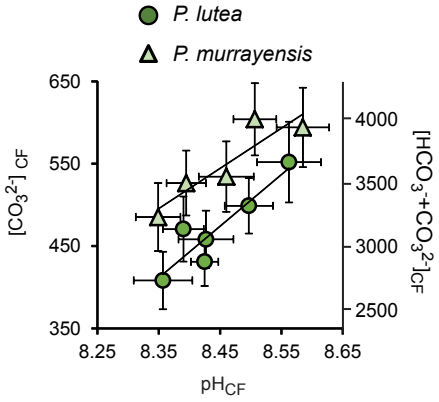

Figure 3. Predicted $[CO_3^{2-}]_{CF}$, $[HCO_3^-]_{CF}$ and $[HCO_3^-+CO_3^{2-}]_{CF}$, assuming the calcification fluid operates as: a-c) an open system in equilibrium with overlying CO_2 of 180, 400 or 750 µatm or d-f) an open system where CO_2 diffusion into the fluid is controlled by ΔC_w. Observed coral data are overlain onto each graph. Symbols denote coral genotypes and colours denote seawater pCO_2 treatment.

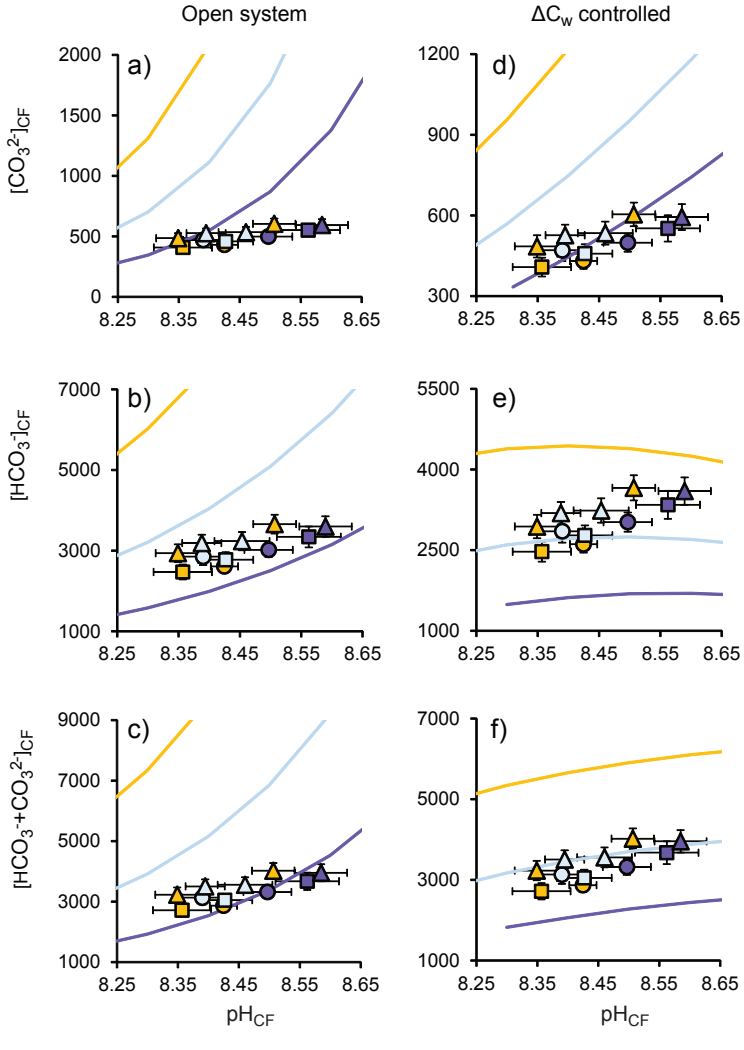

Figure 4. Estimated [CO_2] (µmol kg^{-1}) of a fluid with total [DIC] as in Table 1. Black horizontal lines indicate the [CO_2] of an overlying ambient seawater at a) 180 µatm, b) 400 µatm and c) 750 µatm. These lines are extended across the entire pH_{CF} range to ease visualisation of ΔC_W although the pH of the overlying seawater is constant. ΔC_W indicates the CO_2 concentration gradient between the calcification fluid and ambient seawater at pH 8.5 which facilitates CO_2 diffusion from seawater into the fluid.

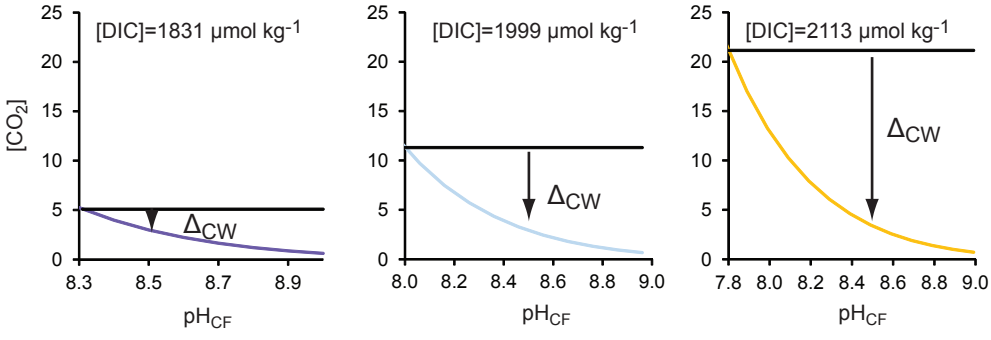

Figure 5. Correlations between coral calcification rate (µmol $CaCO_3$ cm^{-2} day^{-1}) and a) [CO_3^{2-}]$_{CF}$ and [HCO_3^-+CO_3^{2-}]$_{CF}$ and b) [H^+]sw-[H^+]$_{CF}$ for each coral genotype. Coefficients of determination (r^2) for P. lutea 1, P. lutea 2 and P. murrayensis are a) 0.94, 1.00 and 1.00 (excluding the outlier P. murrayensis data point) and b) 0.88, 0.88 and 0.90 (including all data points) respectively. [CO_3^{2-}]$_{CF}$ and [HCO_3^-+CO_3^{2-}]$_{CF}$ error bars are calculated from propagating 95% confidence limits in B/Ca and $\delta^{11}B$ analyses onto DIC system estimates. Calcification rate error bars indicate the standard deviation of multiple (n=3-4) estimates over the 5 week experimental period.